Electronic Supplementary Information

Pore environment reinforced laser dye fluorescence in an adenine-containing metal–organic framework with pocket-like channels

Li-Li Xu, [ac] Hong Cai,*[a] Dong Luo, [b] Mian Li, [c] Yong-Liang Huang, [d] Jie-Ji Zhu,[a] Mo Xie, [b] Zi-Wei Chen,[a] and Dan Li* [b]

[a] School of Chemical and Environmental Engineering, Hanshan Normal University, Chaozhou, Guangdong 521041, P. R. China.

[b] College of Chemistry and Materials Science, Guangdong Provincial Key Laboratory of Functional Supramolecular Coordination Materials and Applications, Jinan University, Guangzhou 510632, P. R. China.

[c] College of Chemistry and Chemical Engineering, Shantou University, and Chemistry and Chemical Engineering Guangdong Laboratory, Guangdong 515063, P. R. China.

[d] Department of Medicinal Chemistry, Shantou University Medical College, Shantou, Guangdong 515041, P. R. China.

* Corresponding author:

E-mail: tiddychen@163.com; danli@jnu.edu.cn

Table of Contents

Experimental Section

Materials and Instruments

All reagents and solvents were purchased from commercial sources and used without further purification. Thermogravimetric analysis (TGA) was carried out in a nitrogen stream using Q50 TGA (TA) thermal analysis equipment with a heating rate of 10 °C/min. Powder X-ray diffraction (PXRD) patterns of the bulk samples were measured on a Rigaku Ultima IV X-ray Diffractometer and Mini Flex 600 Benchtop X-ray diffractometer (Cu Kα, λ = 1.5418 Å). The solid UV-Vis absorption spectra were measured with a Bio-Logic MOS-450/AF-CD spectrometer with KCl pellets. Fourier transform infrared spectra (FTIR) were obtained by KBr disks on a Nicolet Avatar 360 FTIR spectrometer in the range of 4000−400 cm^{-1} (abbreviations for the IR bands: w = weak, m = medium, b = broad, s = strong and vs = very strong). ^{1}H nuclear magnetic resonance (^{1}H NMR) spectra was recorded on Bruker Biospin Avance (400 MHz) equipment. Elemental analysis was carried out with an Elementar vario EL Cube equipment. The steady-state photoluminescence spectra (PL) for all samples were recorded on a PTI QM/TM spectrofluorometer (Birmingham, NJ, USA). Corrections of excitation and emission for the detector response were performed ranging from 200−900 nm. The quantum yields of all samples were measured at room temperature on Hamamatsu C11347-11 (Hamamatsu photonics K.K., Japan). The fluorescence lifetimes of all samples were recorded by an Edinburgh FLS920 spectrometer, which is equipped with a μF900 μs flash lamp. (Edinburgh Instruments Ltd., Livingston, U.K.). Solid-state UV-Vis-NIR diffuse reflection spectra were performed on a Lambda 950 UV/Vis Spectrometer with $BaSO_4$ pellets as the standard (100% reflectance), the finely ground samples from the crystals were coated on the $BaSO_4$ plate. Gas adsorption isotherms were measured with a Micromeritics ASAP2020 gas adsorption instrument. The cryogenic temperature of 77 K required in the sorption of N_2 was controlled by using liquid nitrogen bath. The initial outgassing process for the MeOH-exchanged ZnTDCA-1 and DSM@ZnTDCA-1 were carried out under a high vacuum (less than 10^{-6} mbar) at 120 ℃ for 20 h. The desolvated sample and sample tube were weighed precisely and transferred to the analyzer.

Synthesis of DSM dye

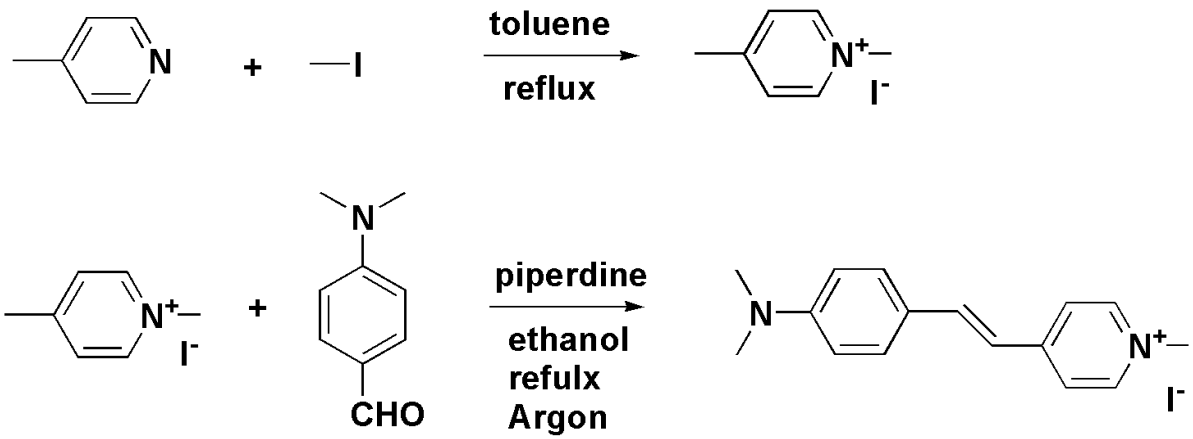

Scheme S1 Synthetic routes of DSM.

The pyridinium hemicyanine dye 4-(*p*-dimethylaminostyryl)-1-methylpyridinium (DSM) was prepared as Scheme S1. (1) 4-Methylpyridine (1.3 g) was dissolved in 35 mL toluene and stirred vigorously while 8.5 g methyl iodide was added dropwise. The resultant mixture reacted at room temperature for 4 h, then was heated up to reflux for 1 h. Finally, the mixture was cool down, filtered, and washed with toluene twice, to get 2.7g white solid of 1, 4-dimethylpyridine iodide salt, with a yield of about 82%. (2) 1, 4-Dimethylpyridine iodized salt (2.3 g) and 4-dimethyl-aminobenaldehyde (1.5 g) were dissolved in 35 mL anhydrous ethanol, 0.2 mL piperidine was added as catalyst. The mixture was stirred for 0.5 h under Ar atmosphere, the solution turned red, and then was refluxed for 12 h, the solution turned red and black, precipitated red solid product. Finally, the mixture was cool down and filtered. The precipitate was washed twice with ice ethanol (about -15 °C), and then recrystallized with ethanol to obtain 2.3 g dark red aciculate crystals of DSM iodide, Yield: ca. 64%. Mp: 261 °C. Elemental analysis of DSM iodide ($C_{16}H_{19}IN_2$, 366.24) calculated (%): C, 52.47; H, 5.23; N, 7.65; found (%): C, 52.57; H, 5.36; N, 7.46. 1H NMR (400 MHz, DMSO-d_6) δ 8.67 (d, J = 6.7 Hz, 2H), 8.04 (d, J = 6.7 Hz, 2H), 7.90 (d, J = 16.1 Hz, 1H), 7.59 (d, J = 8.8 Hz, 2H), 7.16 (d, J = 16.1 Hz, 1H), 6.78 (d, J = 8.8 Hz, 2H), 4.17 (s, 3H), 3.02 (s, 6H) (Fig. S9). FTIR spectrum (KBr pellets, cm^{-1}): 1643 (w), 1578 (vs), 1529 (s), 1508 (s), 1466 (m), 1447 (w), 1433 (m), 1371 (m), 1341 (m), 1316 (m), 1304 (m), 1226 (w), 1164 (vs), 1062 (w), 1040 (w), 982 (m), 941 (w), 871 (w), 825 (m), 536 (w) (Fig. S7).

Synthesis products of DSM@MOF composites

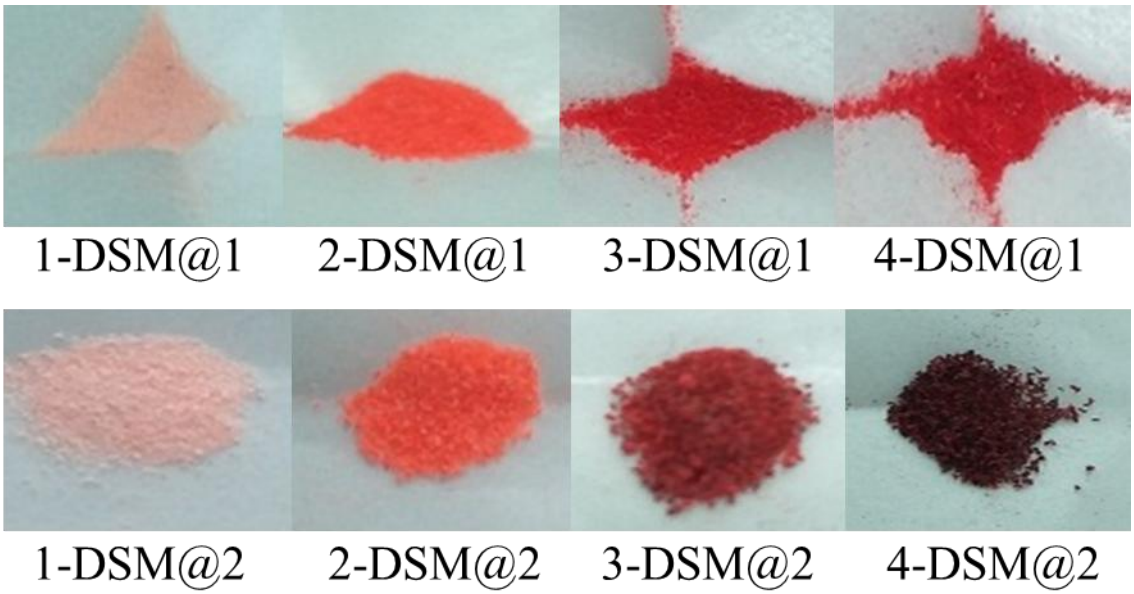

Fig. S1 Images of a series of DSM@1(ZnTDCA-1) and DSM@2(ZnTDCA-2) composites.

Determination of dye contents

Well-dried dye-included crystals of DSM@ZnTDCA-1 or DSM@ZnTDCA-2 (10 mg) were dissolved by concentrated HCl (30 μL), and then diluted using moderate DMF, the DSM content was determined by Fluorescence spectrometry (PL) and UV-Vis spectrophotometry (UV-Vis) respectively. The linear correlation can be fitted by intensity-concentration (0.25–4.00 μmol/L) by PL, or absorbance-concentration (1.00–48.00 μmol/L) by UV-Vis (Fig. S2). The results of DSM content obtained by the two methods were similar (Table S1). Compared with PL, UV-Vis presented a better linear relationship and a wider linear range, but for low content samples, it needed to increase the sample amount for detection. We finally used the results by UV-Vis uniformly.

Table S1 The content of DSM by PL and UV-Vis

Sample	The content of DSM by PL (wt%)	The content of DSM by UV-Vis (wt%)
1-DSM@1	0.01	0.01
2-DSM@1	0.03	0.02
3-DSM@1	0.17	0.15
4-DSM@1	0.79	0.78
1-DSM@2	0.01	0.01
2-DSM@2	0.10	0.10
3-DSM@2	1.01	0.99
4-DSM@2	3.09	3.15

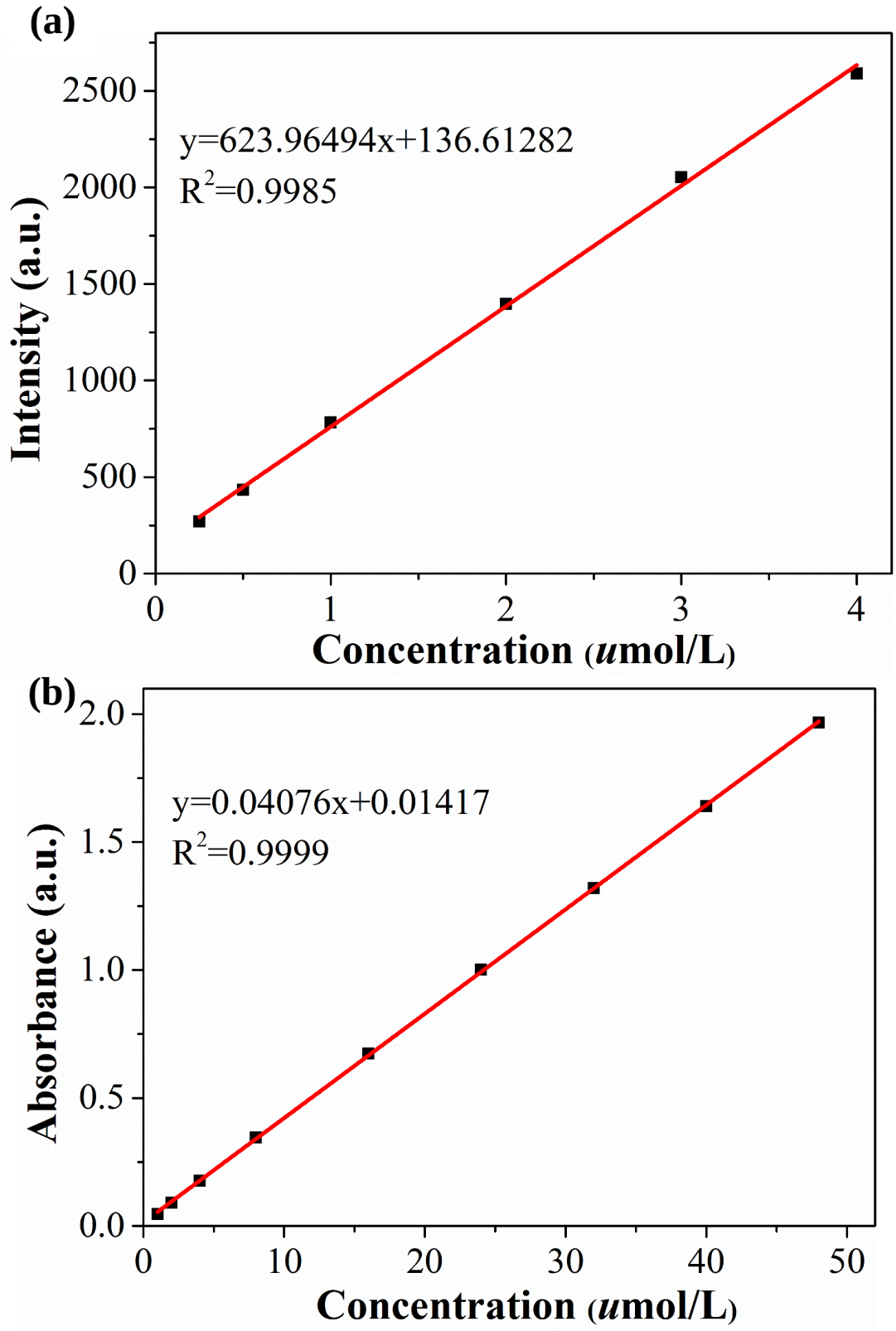

Fig. S2 The standard curve for the DSM solution in DMF by (a) FL (λ_{ex} = 469 nm, λ_{em} = 620 nm) and (b) UV-Vis (λ_{max} = 472 nm).

Crystal Structure Section

Crystal Data and Structure Refinements

A suitable crystal of the complex was mounted with glue at the end of a glass fiber. Data collection was performed with a XtaLAB PRO MM007-DW diffractometer system equipped with a RA-Micro7HF-MR-DW(Cu/Mo) X-ray generator and Pilatus3R-200K-A detector (Rigaku, Japan, Cu Kα, λ = 1.54178 Å). The structure was solved by direct methods and refined by full-matrix least-squares refinements based on F2. Anisotropic thermal parameters were applied to all non-hydrogen atoms. The hydrogen atoms were generated geometrically. The crystallographic calculations were performed using the *SHELXL-2018/3* programs.[1] The treatment for the guest molecules in the cavities of both ZnTDCA-1 and ZnTDCA-2 crystals involve the use of the SQUEEZE program of PLATON.[2] Crystal data and structure refinement parameters are summarized in Table S2. CCDC Nos. 2225750-2225751.

Table S2 Crystal data and refinement parameters for ZnTDCA-1 and ZnTDCA-2

	ZnTDCA-1	**ZnTDCA-2**
Empirical formula	$C_{61}H_{41}N_{30}O_{25}S_5Zn_8$	$C_{28}H_{15}N_{10}O_{13}S_3Zn_4$
Formula weight	2277.50	1057.16
Temperature(K)	100.15	100.15
Crystal system	Monoclinic	Tetragonal
space group	*C*2/*c*	*I*4/*mmm*
***a* (Å)**	42.9603(4)	34.1984(7)
***b* (Å)**	17.2625(2)	34.1984(7)
***c* (Å)**	15.2664(2)	13.3670(4)
***a* =*γ* (°)**	90	90
***β* (°)**	106.9427(9)	90
Volume (Å^3)	10830.2(2)	15633.1(8)
Z	4	8
ρ_{calc}（g cm^{-3}）	1.397	0.898
***F*(000)**	4548.0	4200.0
***μ* (mm^{-1})**	3.452	2.471
Reflections collected	29014	19118
Unique reflections	9024	4261
R_{int}	0.0192	0.0237
Data / restraints / parameters	9024/433/705	4261/285/192
GOOF on F^2	1.105	1.044
R_1[I≥2σ(I)]^a	0.0526	0.0676
wR_2[I≥2σ(I)]^b	0.1190	0.1984
R_1[all data]^a	0.0545	0.0860
wR_2[all data]^b	0.1200	0.2260
Largest diff. peak/hole / e Å^{-3}	0.94, -0.79	0.87, -0.55
CCDC number	2225750	2225751

^{a} $R_1 = \Sigma\,(||F_0|- |F_c||)/\Sigma|F_0|$; ^{b} $wR_2 = [\Sigma w\,(F_0^2 - F_c^2)^2/\Sigma w(F_0^2)^2]^{1/2}$

Topological Analysis

Methods: *Systre*[3] program and the commercial software *CrystalMaker X* were used to identify the underlying net of MOFs and to generate/process the .cgd file for the nets. *ToposPro*[4] program was used for computing point symbol and vertex symbol[5] of the net. The *RCSR* (Reticular Chemistry Structure Resource)[6] and *Topcryst* (The Samara Topological Data Center)[7] online databases can be used for searching nets and checking their occurrences in crystal structures.

Systre files for the new net

CRYSTAL
 NAME ZnTDCA-1
 GROUP C12/c1
 CELL 4.11364 2.31062 2.03151 90.0000 91.0077 90.0000
 NODE 1 6 0.08537 0.05093 0.33137
 NODE 2 4 0.44678 0.14954 0.02406
 NODE 3 4 0.31775 0.18246 0.34002
 EDGE 0.44678 0.14954 0.02406 0.31775 -0.18246 -0.15998
 EDGE 0.08537 0.05093 0.33137 0.05322 0.35046 -0.02406
 EDGE 0.08537 0.05093 0.33137 0.05322 -0.35046 0.47594
 EDGE 0.08537 0.05093 0.33137 0.18225 0.31754 0.65998
 EDGE 0.08537 0.05093 0.33137 0.31775 0.18246 0.34002
 EDGE 0.08537 0.05093 0.33137 -0.08537 -0.05093 0.66863
 EDGE 0.44678 0.14954 0.02406 0.55322 0.14954 0.47594
 EDGE 0.08537 0.05093 0.33137 0.18225 -0.31754 0.15998
EDGE_CENTER 0.38226 -0.01646 -0.06796
EDGE_CENTER 0.06930 0.20069 0.15365
EDGE_CENTER 0.06930 -0.14976 0.40365
EDGE_CENTER 0.13381 0.18423 0.49567
EDGE_CENTER 0.20156 0.11670 0.33570
EDGE_CENTER 0.00000 0.00000 0.50000
EDGE_CENTER 0.50000 0.14954 0.25000
EDGE_CENTER 0.13381 -0.13330 0.24567

END

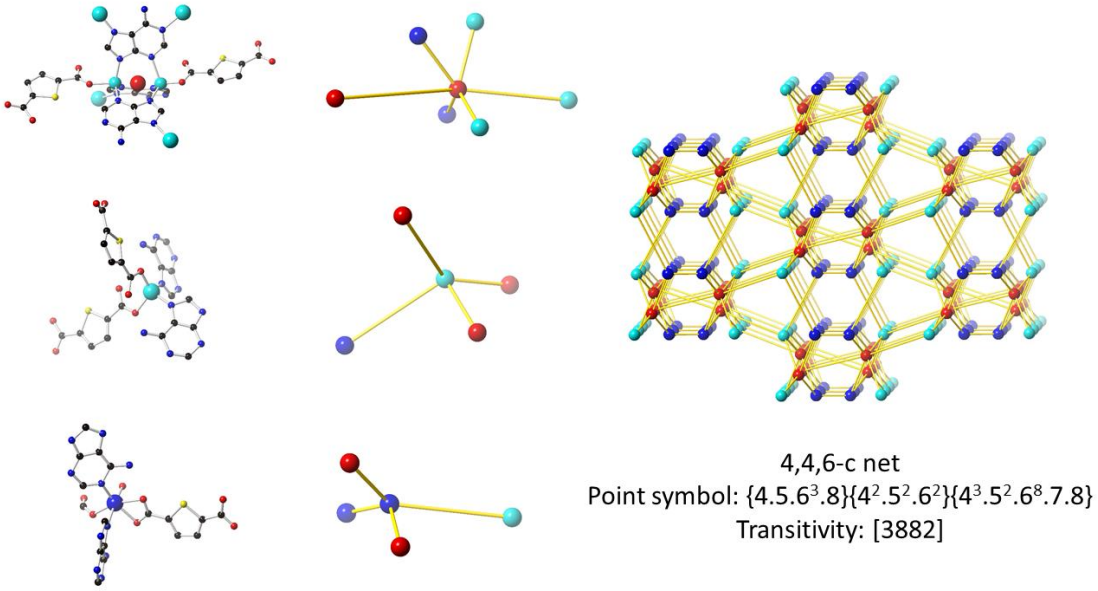

Fig. S3 Underlying topological network of ZnTDCA-1, where the red balls, cyan balls and blue balls represent $Zn_2(COO)_2(Ade)_3$ paddlewheel clusters, $Zn(COO)_2(Ade)_2$ clusters and ZnO(η^1-COO) (η^2-COO) $(Ade)_2$ clusters, respectively.

From the topological point of view, $Zn(COO)_2(Ade)_2$ and ZnO(η^1-COO) (η^2-COO)$(Ade)_2$ act as two 4-connected nodes, while $Zn_2(COO)_2(Ade)_3$ acts as a 6-connected node (see Fig. S3 left and middle). Thus, the framework can be simplified as a trinodal 4,4,6-c net with the point symbol of $\{4.5.6^3.8\}\{4^2.5^2.6^2\}\{4^3.5^2.6^8.7.8\}$, transitivity: [3882], which is a new topological net checked by Systre and ToposPro.[3,4]

Systre files for the new net

CRYSTAL

NAME ZnTDCA-2

GROUP P4/mmm

CELL 5.34533 5.34533 0.50431 90.0000 90.0000 90.0000

NODE 1 3 0.00000 0.31281 0.00000

NODE 3 4 0.00000 0.13216 0.50000

NODE 4 4 0.00000 0.50000 0.00000

EDGE 0.00000 0.13216 0.50000 0.13216 0.00000 0.50000

EDGE 0.00000 0.50000 0.00000 0.00000 0.50000 2.00000

EDGE 0.00000 0.31281 0.00000 0.00000 0.13216 0.50000

EDGE 0.00000 0.31281 0.00000 0.00000 0.50000 0.00000

EDGE_CENTER 0.06608 0.06608 0.50000

EDGE_CENTER 0.00000 0.50000 1.00000

EDGE_CENTER 0.00000 0.22248 0.25000

EDGE_CENTER 0.00000 0.40641 0.00000

END

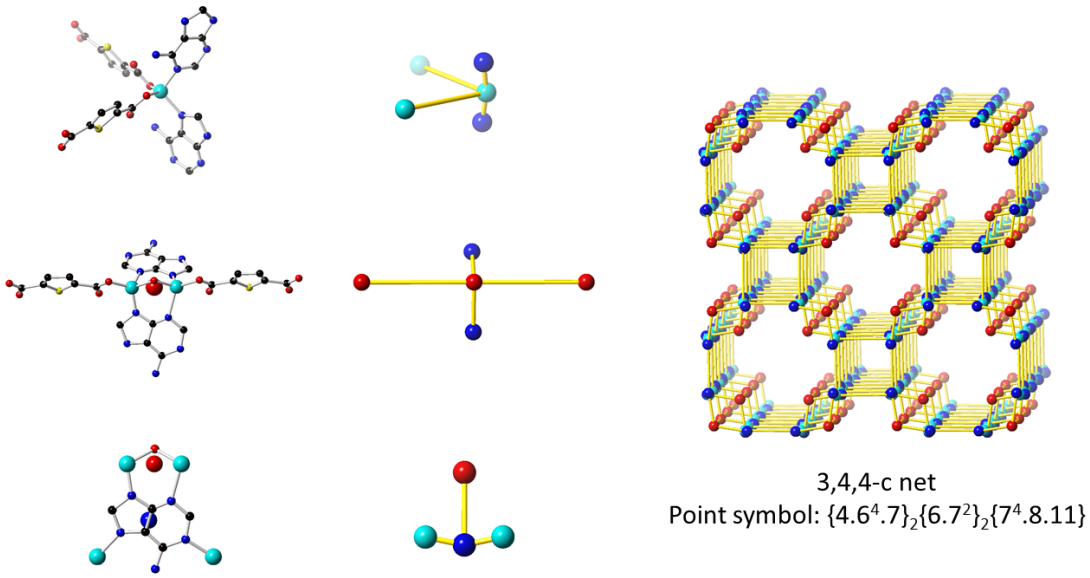

Fig. S4 Underlying topological network of ZnTDCA-2, where the cyan balls and red balls represent $Zn(COO)_2(Ade)_2$ and $Zn_2O(COO)_2(Ade)_2$ coordination nodes, respectively, and blue balls represent Adenine ligands.

From the topological point of view, $Zn(COO)_2(Ade)_2$ and $Zn_2O(COO)_2(Ade)_2$ can be simplified to two different 4-connected nodes (see Fig. S4 left and middle), and adenine ligand acts as a 3-connected node. Thus, the total framework can be simplified as a (3,4,4)-c net with the point symbol of $\{4.6^4.7\}\{6.7^2\}_2\{7^4.8.11\}$, which is a new topological net checked by Systre and ToposPro. [3,4]

Hydrogen bonding and voids in the 3D frameworks

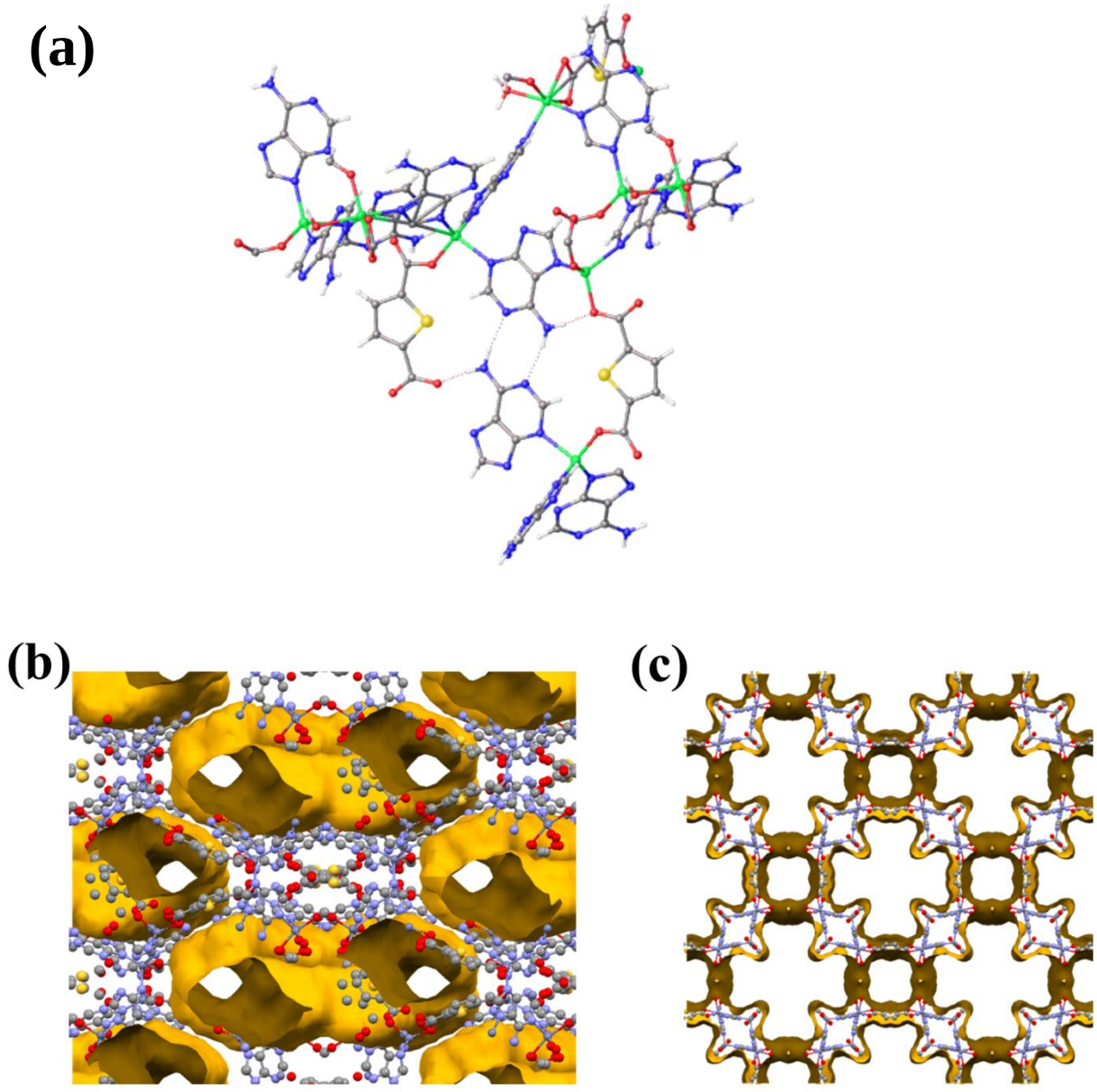

Fig. S5 (a) Hydrogen bonding at the Watson-Crick site of adenine in ZnTDCA-1. Voids in the 3D frameworks of (b) ZnTDCA-1 and (c) ZnTDCA-2 along *c* axis by Mercury (probe radius:1.2 Å).

Physical Measurements

ZnTDCA-1, ZnTDCA-2 and related ligands (H_2TDC, Ade) were characterized by FTIR spectra (Fig. S6–S7). FTIR analysis of ZnTDCA-1 (or ZnTDCA-2) reveals the characteristic peaks of related ligands. The structural components of ZnTDCA-1, ZnTDCA-2, DSM were also proved by ^{1}H NMR spectra (Fig. S8–S9). The peaks of related ligands exist in the ^{1}H NMR spectra of ZnTDCA-1and ZnTDCA-2 and showed the mole ratio of Ade and H_2TDC was 1:0.82 in ZnTDCA-1, and 1:1.49 in ZnTDCA-2. These are consistent with their single crystal structures (6:5 and 1:1.5, respectively).

The powder X-ray diffraction (PXRD) measurements revealed that the bulk ZnTDCA-1 and ZnTDCA-2 closely matched the simulated patterns generated from the results of single-crystal diffraction data, respectively. ZnTDCA-1 and ZnTDCA-2 showed different thermal stability and solvent resistance (Fig. S10-S14). The N_2 adsorption-desorption, DFT pore size distribution of ZnTDCA-1 and DSM@ZnTDCA-1 indicated DSM had been successfully encapsulated into ZnTDCA-1 (Fig. S15). The UV-Vis spectra of ZnTDCA-1 and ZnTDCA-2 exhibited similar features with related ligands, due to the $\pi \rightarrow \pi^*$ and $n \rightarrow \pi^*$ transitions of the H_2TDC and Ade molecules (Fig. S16).[8] The luminescence and ultraviolet absorption behaves of DSM, Ade, H_2TDC, **1** (ZnTDCA-1), **2** (ZnTDCA-2), a series of DSM@ZnTDCA-1 composites and DSM@ZnTDCA-2 composites were showed in Fig. S16-S21. The lifetime, energy transfer efficiency, quantum yield of DSM, ZnTDCA-1, ZnTDCA-2, DSM@ZnTDCA-1 and DSM@ZnTDCA-2 showed in Tables S3–S4. The DSM release experiments, cell culture and cytotoxicity experiments, DFT computation were showed in Fig. S22-S24, respectively.

FTIR

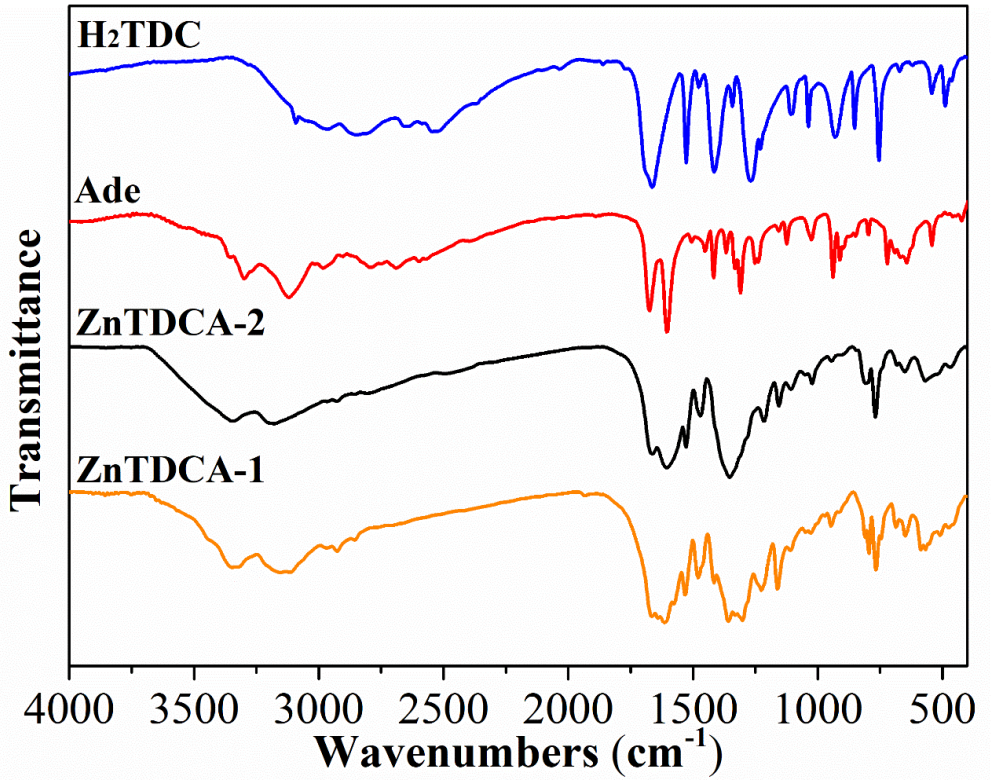

Fig. S6 FTIR spectra of Ade, H_2TDC and ZnTDCA-1 and ZnTDCA-2.

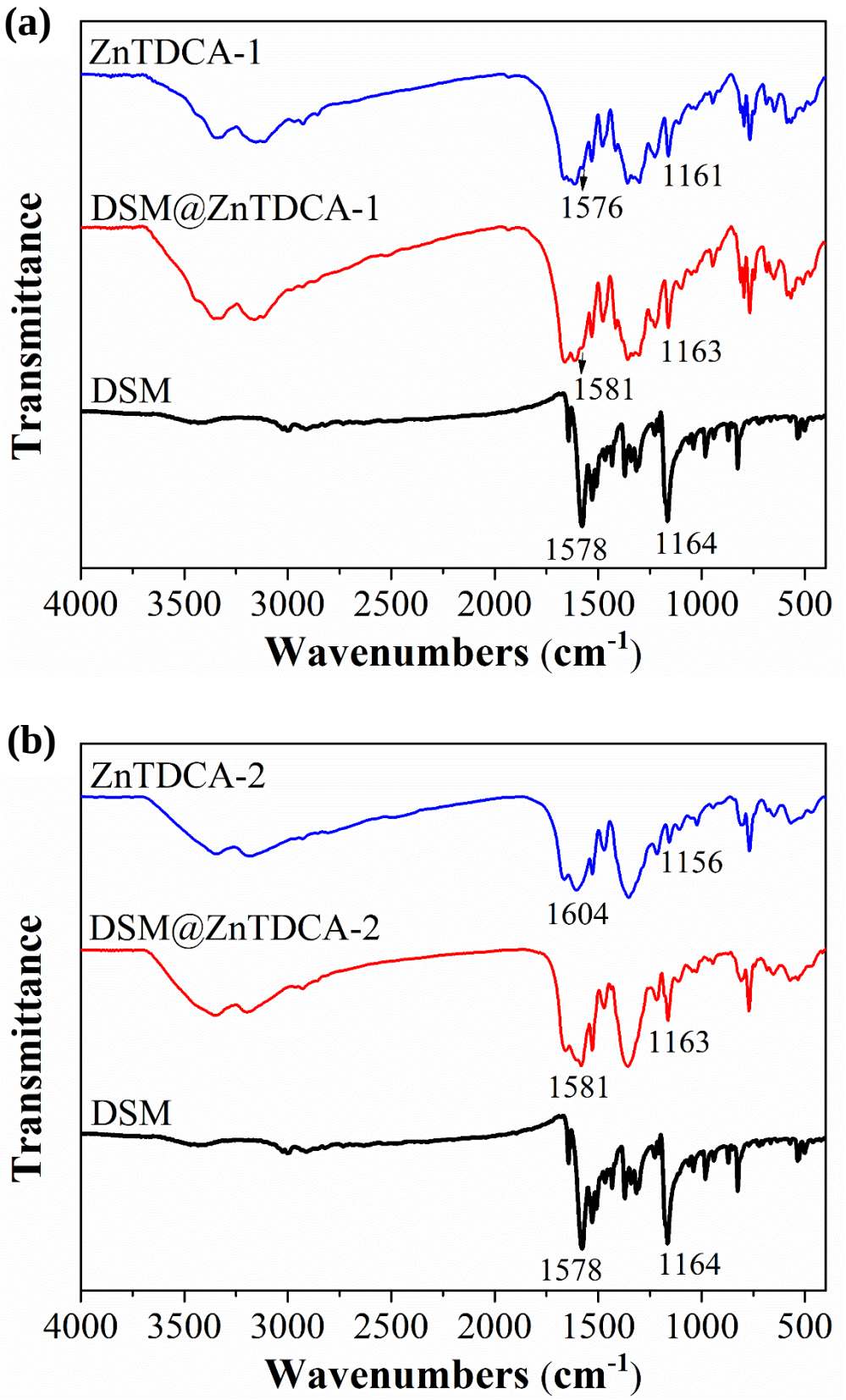

Fig. S7 Comparation of FTIR of (a) ZnTDCA-1 and (b) ZnTDCA-2 before and after immersing in DSM solution (1×10^{-3} mol/L).

^{1}H NMR

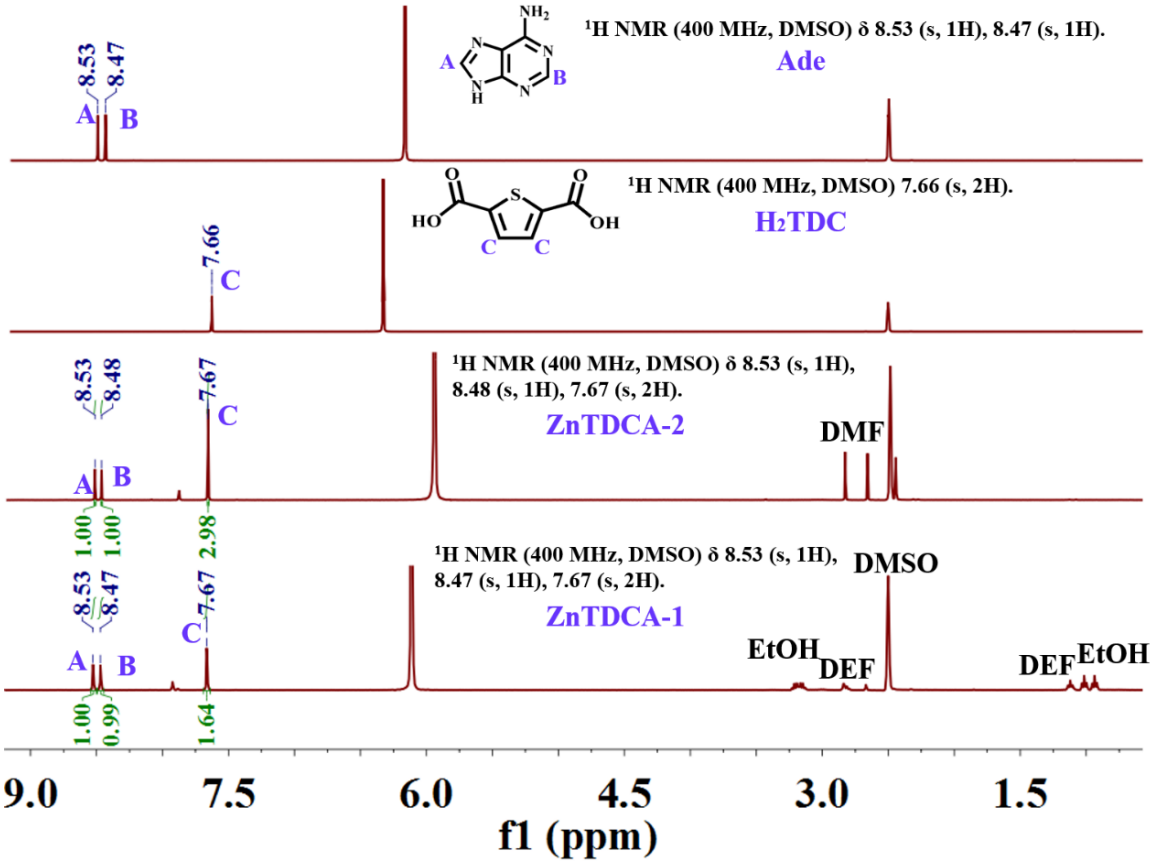

Fig. S8 ^{1}H NMR spectra of ZnTDCA-1, ZnTDCA-2 and related ligands in DMSO-d_6 and 3 drops of DCl (which were used to disolved complex) at 298 K.

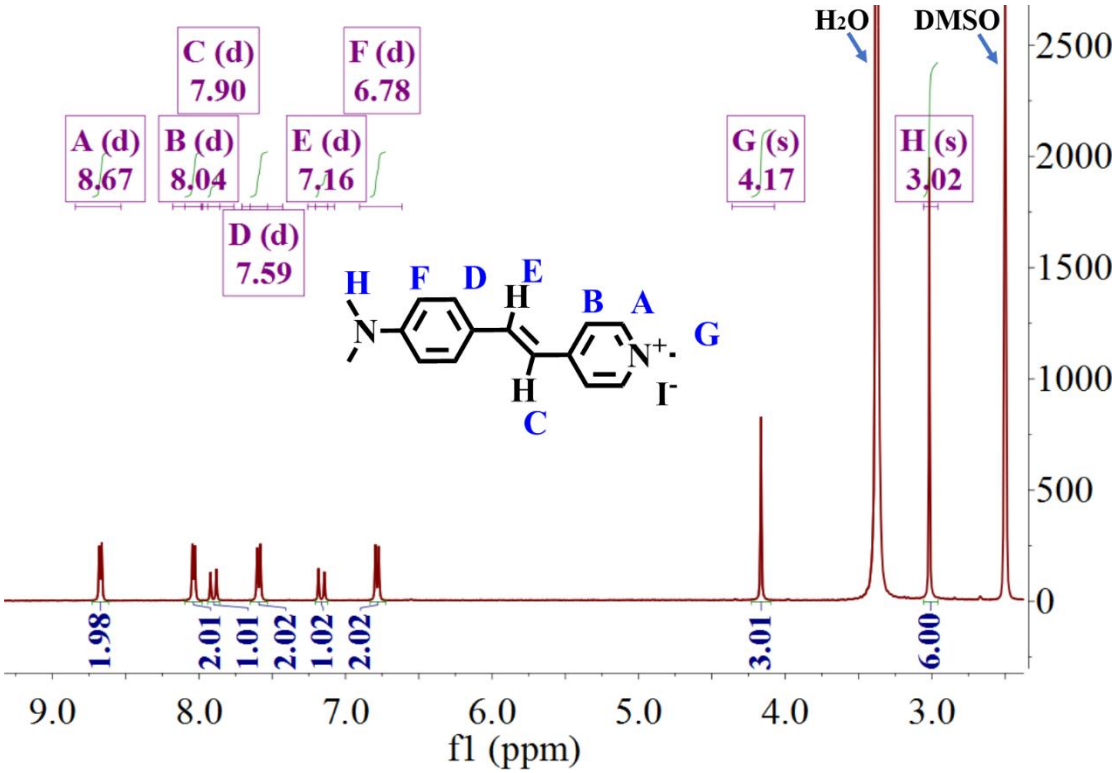

Fig. S9 ^{1}H NMR spectrum of DSM in DMSO-d_6 at 298 K.

PXRD

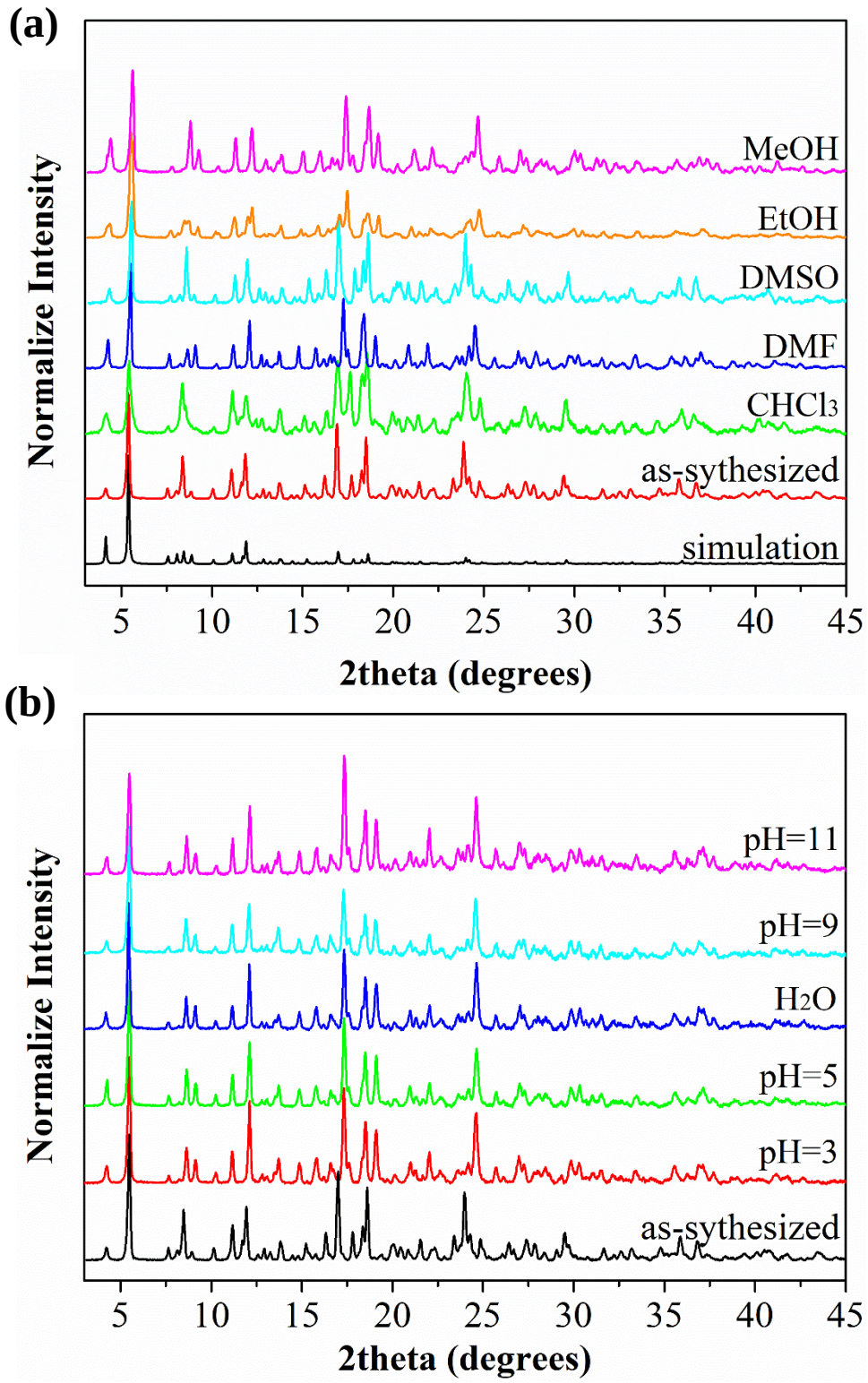

Fig. S10 PXRD patterns of the as-synthesized ZnTDCA-1 before and being soaked in different solvents (a) and aqueous solution of pH 3-11 (b) for a week at room temperature. (DMSO: Dimethyl sulfoxide; DMF: N,N-Dimethylformamide).

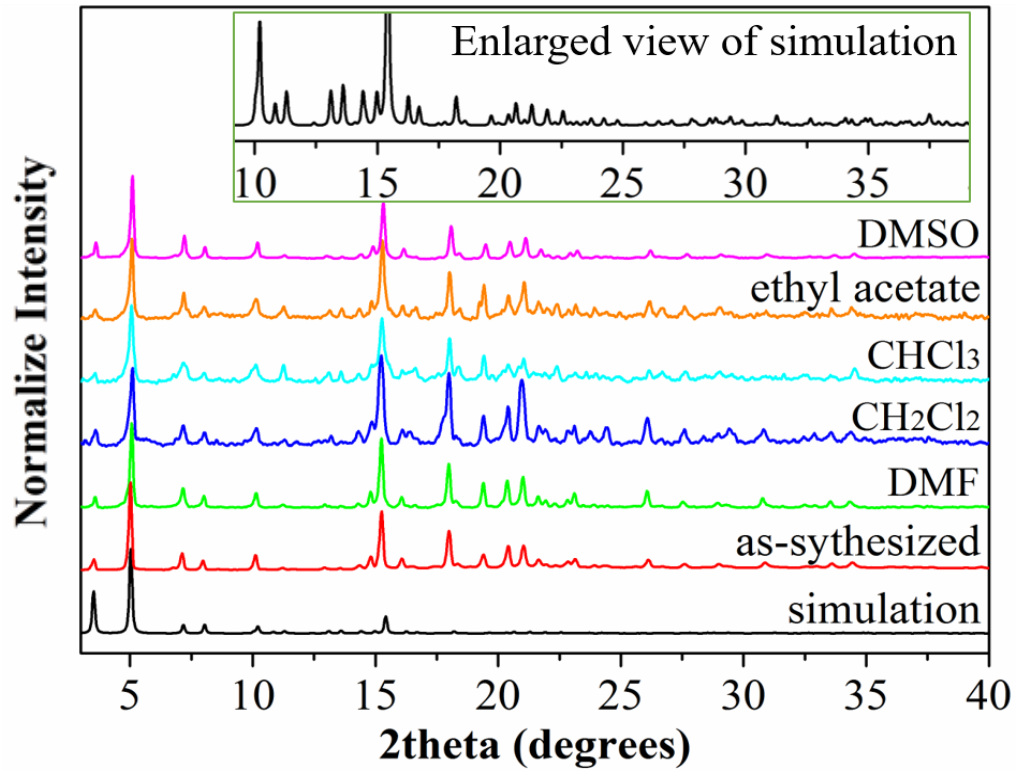

Fig. S11 PXRD patterns of the as-synthesized ZnTDCA-2 and ZnTDCA-2 after being soaked in different solvents for four days at room temperature. The small variations in the PXRD pattern may be due to guest molecule interaction.

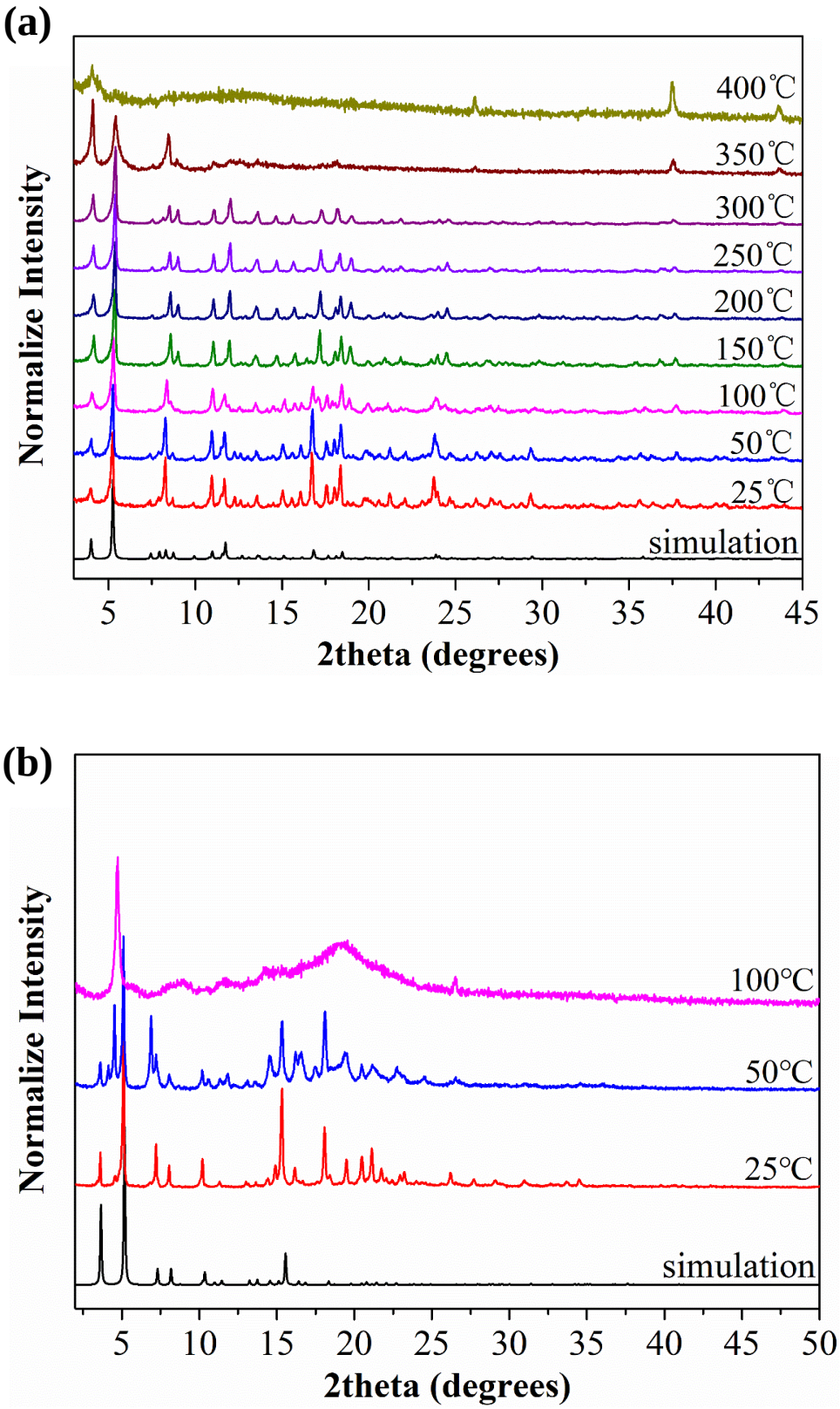

Fig. S12 Powder X-ray diffraction pattern (PXRD) of (a) ZnTDCA-1 and (b) ZnFDCA-2 as-synthesized sample and heated in the air. The small variations in the PXRD pattern may result from the loss of guest molecules.

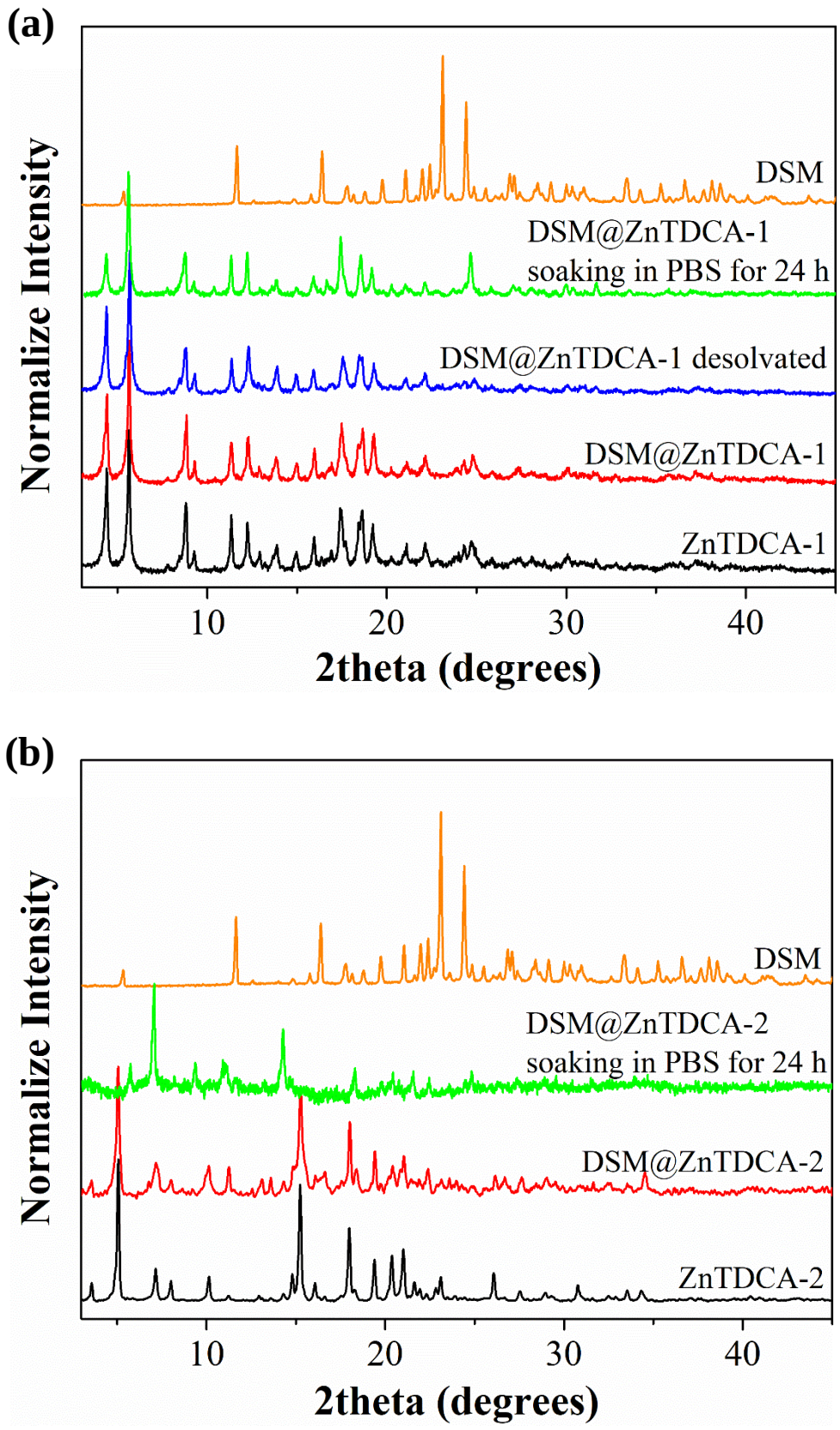

Fig. S13 Comparation of PXRD of (a) ZnTDCA-1 and (b) ZnTDCA-2 before and after immersing in DSM/DMF solution (1×10^{-3} mol/L) and PBS solution.

TGA

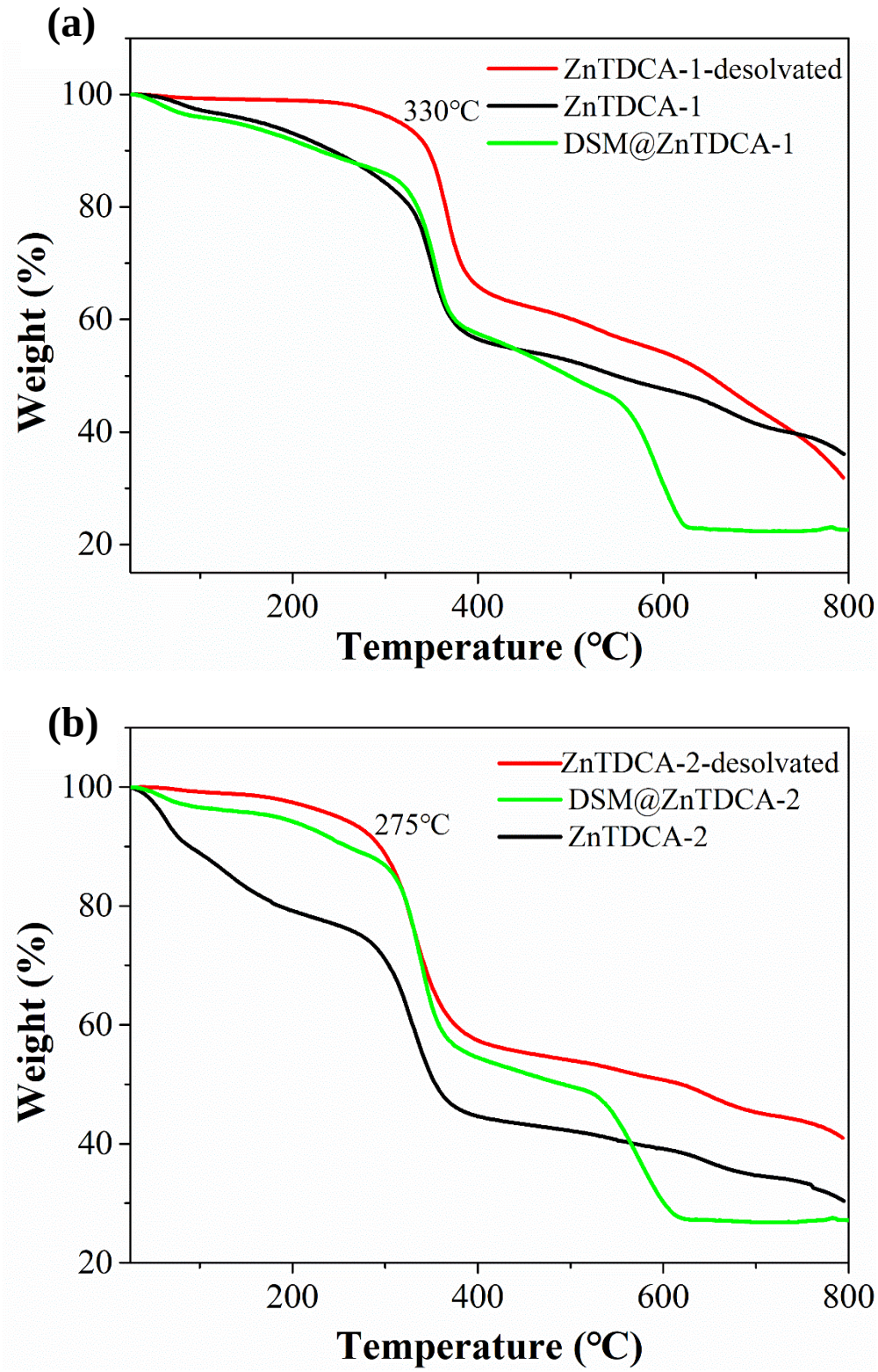

Fig. S14 TGA plots of ZnTDCA-1 (a) and ZnFDCA-2 (b) after different pre-processing: as synthesized (black), desolvated (red), ZnTDCA-1 packaging 0.78 wt % DSM and ZnFDCA-2 packaging 3.15 wt % DSM (green).

N_2 Adsorption

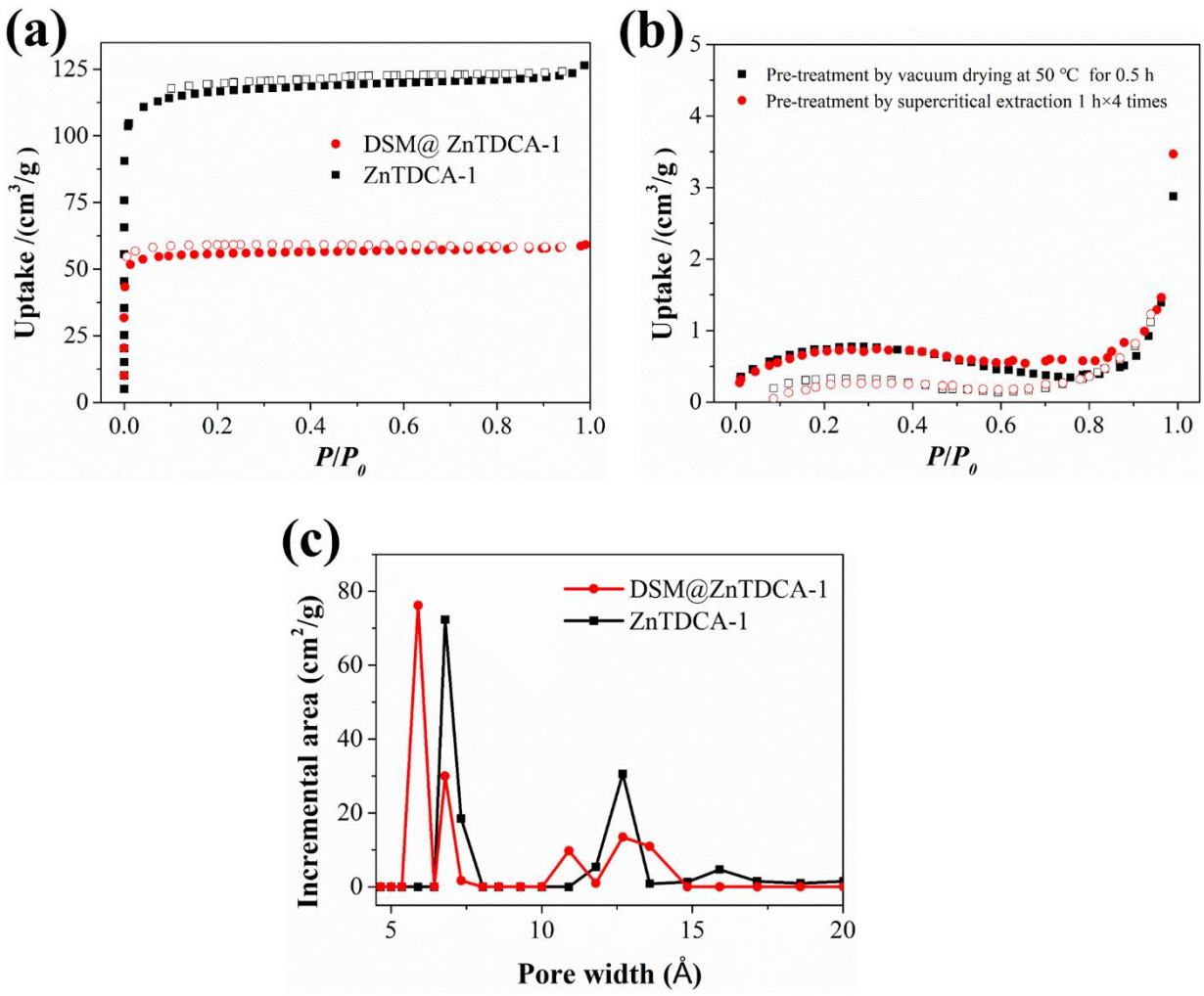

Fig. S15 Comparison of the N_2 adsorption-desorption isotherms (a) ZnTDCA-1 (black) and DSM@ZnTDCA-1 (red) at 77 K. (b) Comparison of the N_2 adsorption-desorption isotherms of ZnTDCA-2 at 77 K. Black: pre-treatment by vacuum drying at 50 °C for 0.5 h. Red: pre-treatment by supercritical extraction 1 h × 4 times. (c) DFT pore size distribution plots of ZnTDCA-1 (black) and DSM@ZnTDCA-1 (red).

Solid-State UV-Vis Absorption Spectra

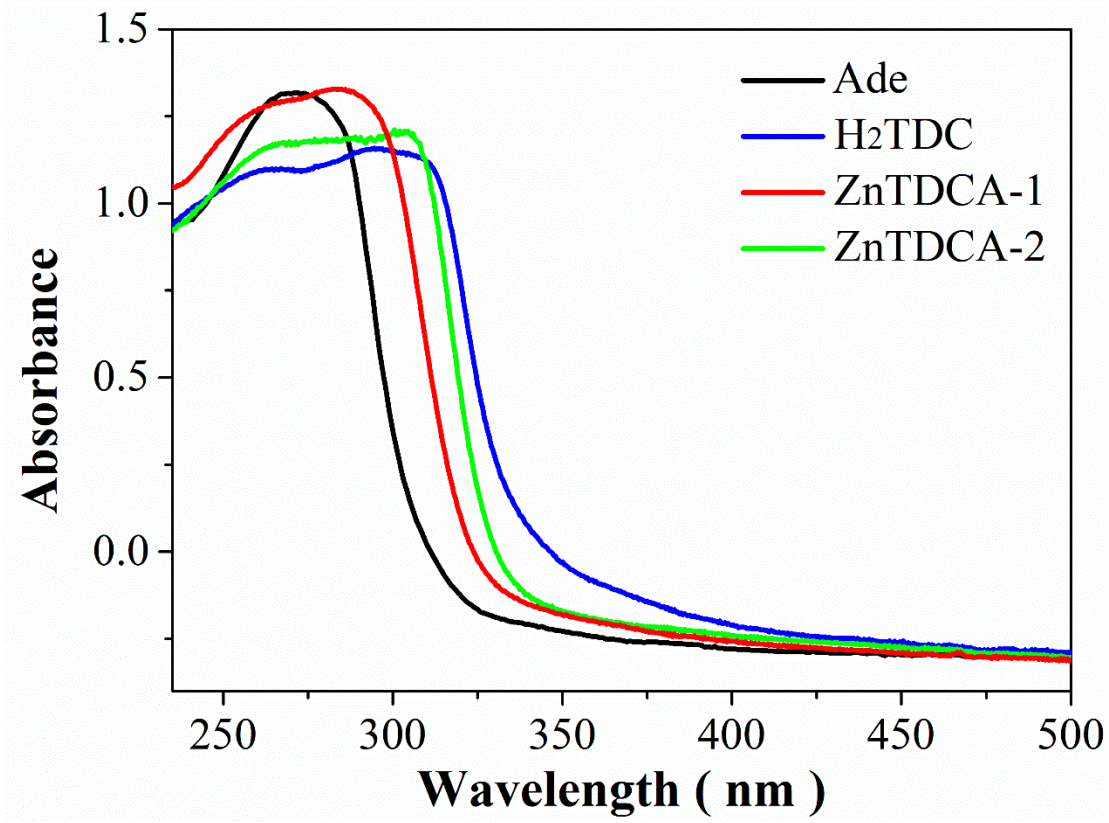

Fig. S16 Solid-state UV-Vis absorption spectra of ZnTDCA-1 (red), ZnTDCA-2 (green), 2,5-thiophenedicarboxylic acid (blue) and adenine (black) at room temperature.

Photoluminescence

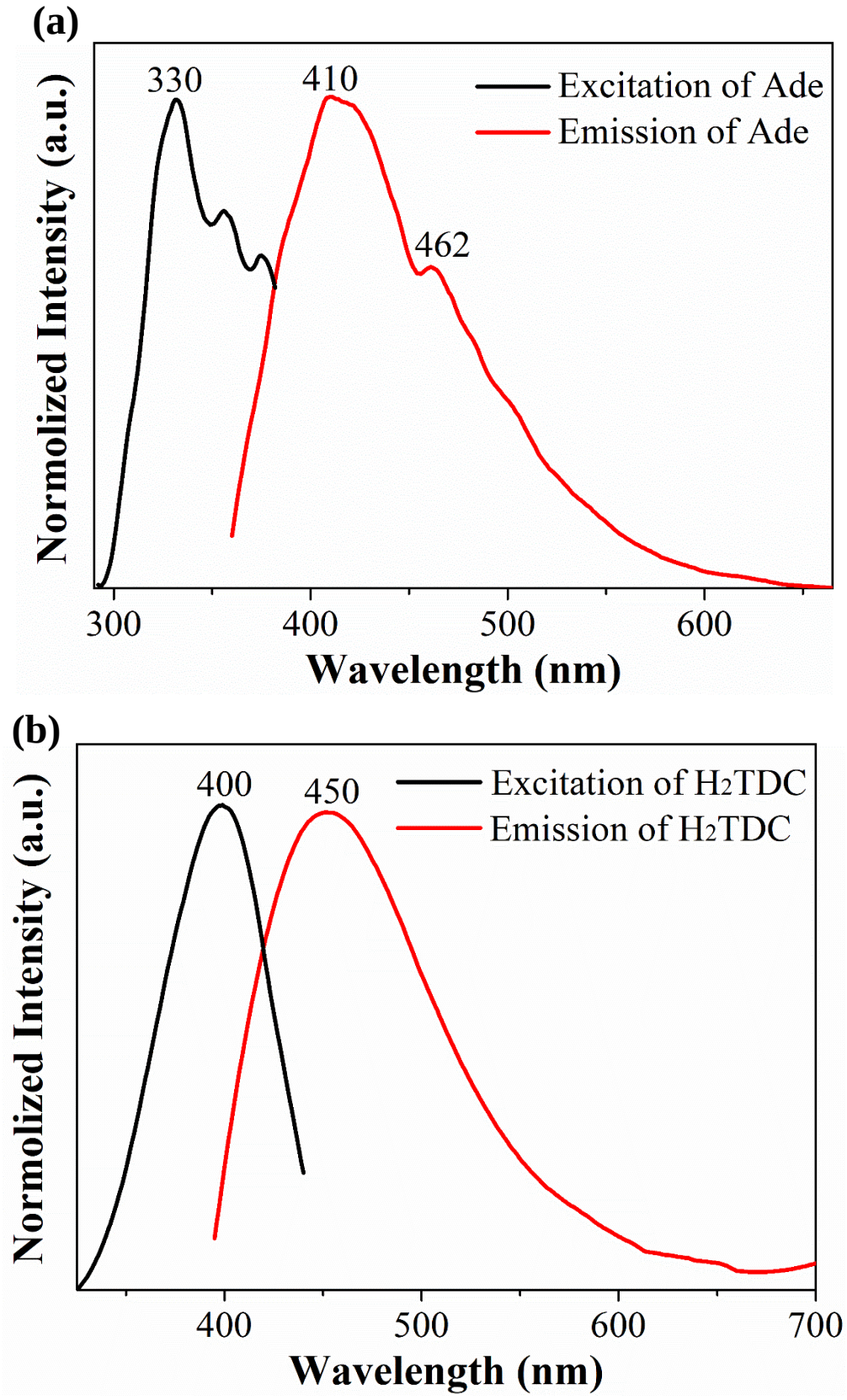

Fig. S17 The excitation (black) and emission (red) spectra of (a) Adenine and (b) 2,5-thiophenedicarboxylic acid in the solid state at room temperature.

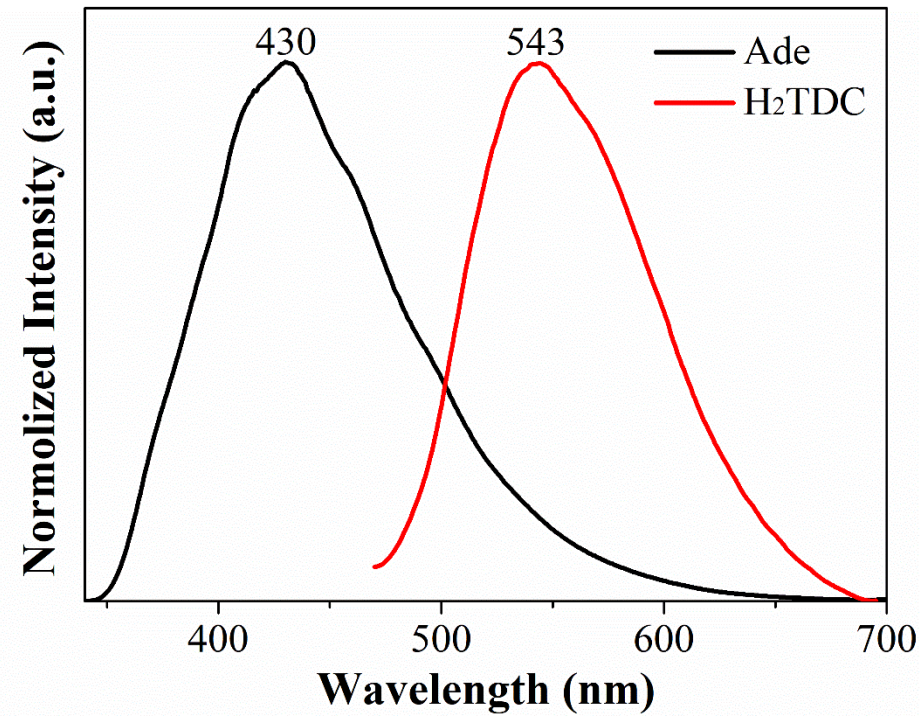

Fig. S18 The emission spectra of (a) Adenine (black) and (b) 2,5-thiophenedicarboxylic acid (red) in the solid state at 78K (the unified excitation wavelength is 320 nm).

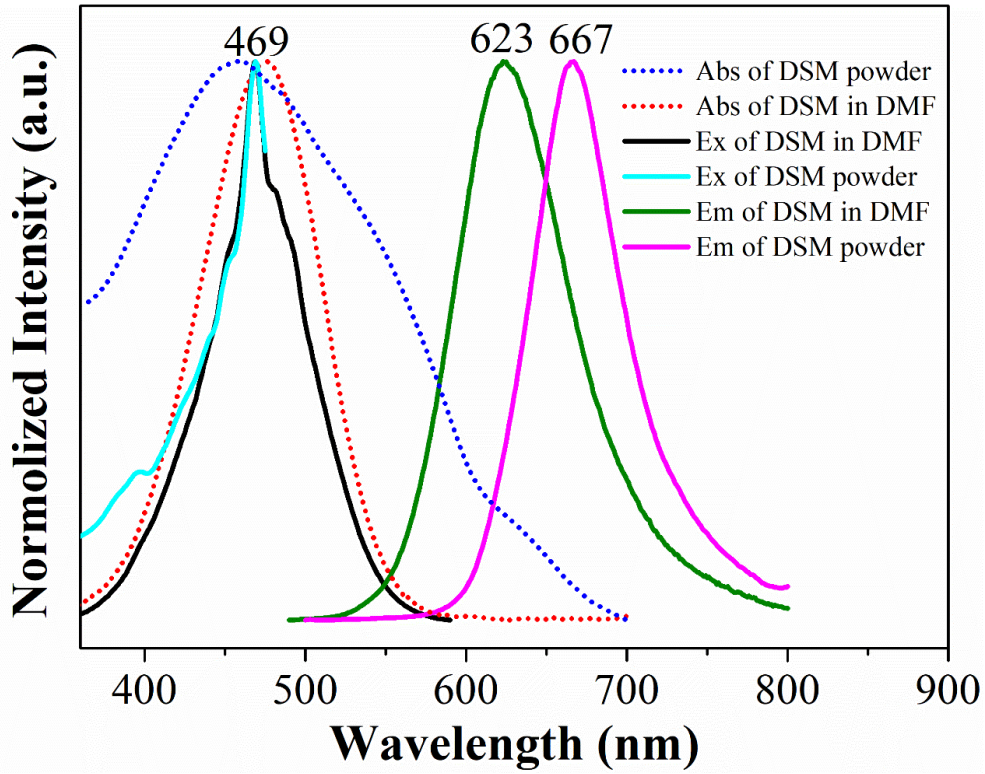

Fig. S19 The excitation, emission and UV-Vis absorption spectra of DSM powder and DSM in DMF solution (1.0×10^{-6} mol/L).

CIE Chromaticity Diagram

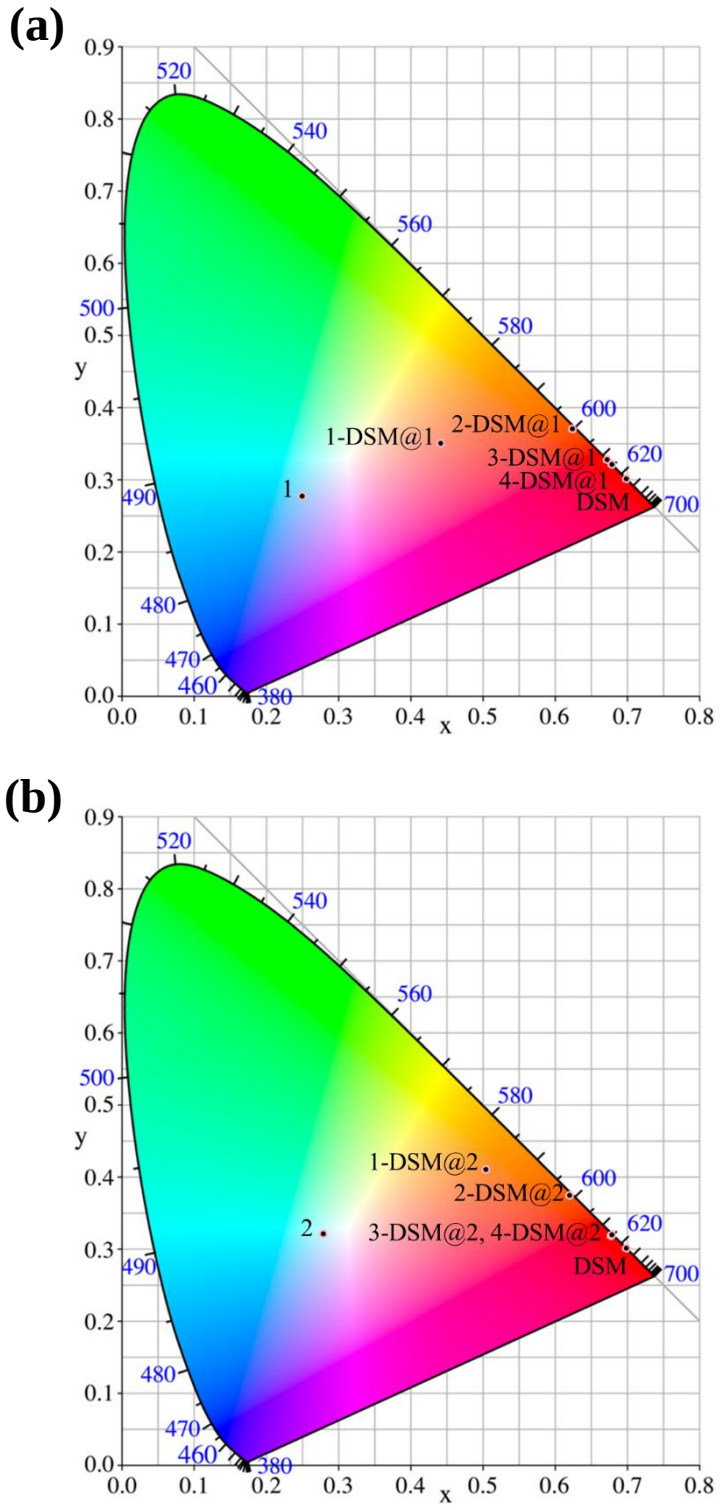

Fig. S20 CIE chromaticity diagram showing the luminescence colors of (a) DSM, **1** (ZnTDCA-1) and a series of DSM@ZnTDCA-1 composites; (b) DSM, **2** (ZnTDCA-2) and a series of DSM@ZnTDCA-2 composites (the CIE chromaticity of 3-DSM@2 and 4-DSM@2 basically overlapped; the unified excitation wavelength is 340 nm).

Lifetime Fitting

Table S3. Fitting data of the photoluminescence decay of samples

Sample	λ_{em}/nm	α_1	α_2	α_3	τ_1/ns	τ_2/ns	τ_3/ns	$<\tau_{av}>$/ns	Chi2
1(ZnTDCA-1)	425	0.840	0.160		1.21	4.81		1.79	0.64
1-DSM@1	414	0.655	0.345		0.36	2.23		1.01	1.10
	600	0.851	0.149		2.41	6.49		3.02	0.73
2-DSM@1	414	0.792	0.208		0.51	2.30		0.88	0.77
	610	1.000			2.46			2.46	0.72
3-DSM@1	414	0.581	0.354	0.065	0.06	0.76	2.48	0.47	1.21
	623	1.000	0.000		1.90			1.90	0.85
4-DSM@1	414	0.015	0.985		4.57	0.06		0.13	1.16
	627	1.000	0.000		1.75			1.75	0.82
2(ZnTDCA-2)	435	0.563	0.398	0.040	1.19	2.35	7.91	1.92	1.11
1-DSM@2	414	0.534	0.330	0.137	0.25	1.60	6.88	1.60	1.13
	596	0.914	0.086		2.87	7.97		3.30	0.92
2-DSM@2	414	0.736	0.226	0.039	0.18	1.16	4.77	0.58	0.93
	610	1.000	0.000		2.86			2.86	0.71
3-DSM@2	414	0.916	0.064	0.020	0.05	1.25	4.27	0.21	1.58
	637	0.613	0.387		0.76	2.85		1.57	0.84
4-DSM@2	414	0.030	0.960	0.010	1.66	0.02	6.27	0.13	1.63
	667	0.603	0.397		0.73	2.64		1.49	1.26

The emission peaks of 414–435nm were attributable to MOF frameworks, while 596–667nm were assigned to the emission of DSM guest. The amplitude-weighted average fluorescence lifetimes were calculated based on the following equation (**1**),[9,10] where τ and α are lifetime and amplitude, respectively.

$$< \tau_{av} >= \sum_i a_i \tau_i \qquad (\mathbf{1})$$

A summary of the energy transfer efficiency and quantum yield

Φ_{ET} was calculated based on the following equation (2): [10,11]

$$\emptyset_{ET} = \frac{k_e}{k_r+k_{nr}+k_e} = \frac{k_e}{k_0+k_e} = 1 - \frac{\tau_{DSM@MOF}}{\tau_{MOF}} \qquad (2)$$

where k_r, k_{nr}, and k_e are on behalf of radiative decay, nonradiative decay, and energy transfer constants, respectively. The k_0 and k_e values are found from the lifetime for donor molecule (τ_{MOF}) and donor molecule in the presence of acceptor ($\tau_{DSM@MOF}$), where $\tau_{MOF} = 1/k_0$ and $\tau_{DSM@MOF} = 1/ (k_0+ k_e)$, respectively.

Table S4. The lifetime, energy transfer efficiency, quantum yield of DSM, ZnTDCA-1, ZnTDCA-2, DSM@ZnTDCA-1 and DSM@ZnTDCA-2 with different DSM content

Name	The content of DSM in DSM@MOF (%)	Lifetime of MOF in DSM@MOF (ns)	Lifetime of DSM in DSM@MOF (ns)	Energy transfer efficiency (Φ_{ET}) %[a]	Quantum yield (%)
DSM					2.1
1	0	1.79			2.0
1-DSM@1	0.01	1.01	3.02	43.50%	4.1
2-DSM@1	0.02	0.88	2.46	50.69%	29.9
3-DSM@1	0.15	0.47	1.90	73.77%	38.0
4-DSM@1	0.78	0.13	1.75	92.86%	39.3
2	0	1.92			2.4
1-DSM@2	0.01	1.60	3.30	16.55%	5.1
2-DSM@2	0.10	0.58	2.86	51.35%	39.9
3-DSM@2	0.99	0.21	1.57	89.11%	17.0
4-DSM@2	3.15	0.13	1.49	93.01%	4.7

[a] The excitation wavelength of the quantum yield was 340 nm, except for DSM (at 470 nm)

Fluorescent Microscopic Images

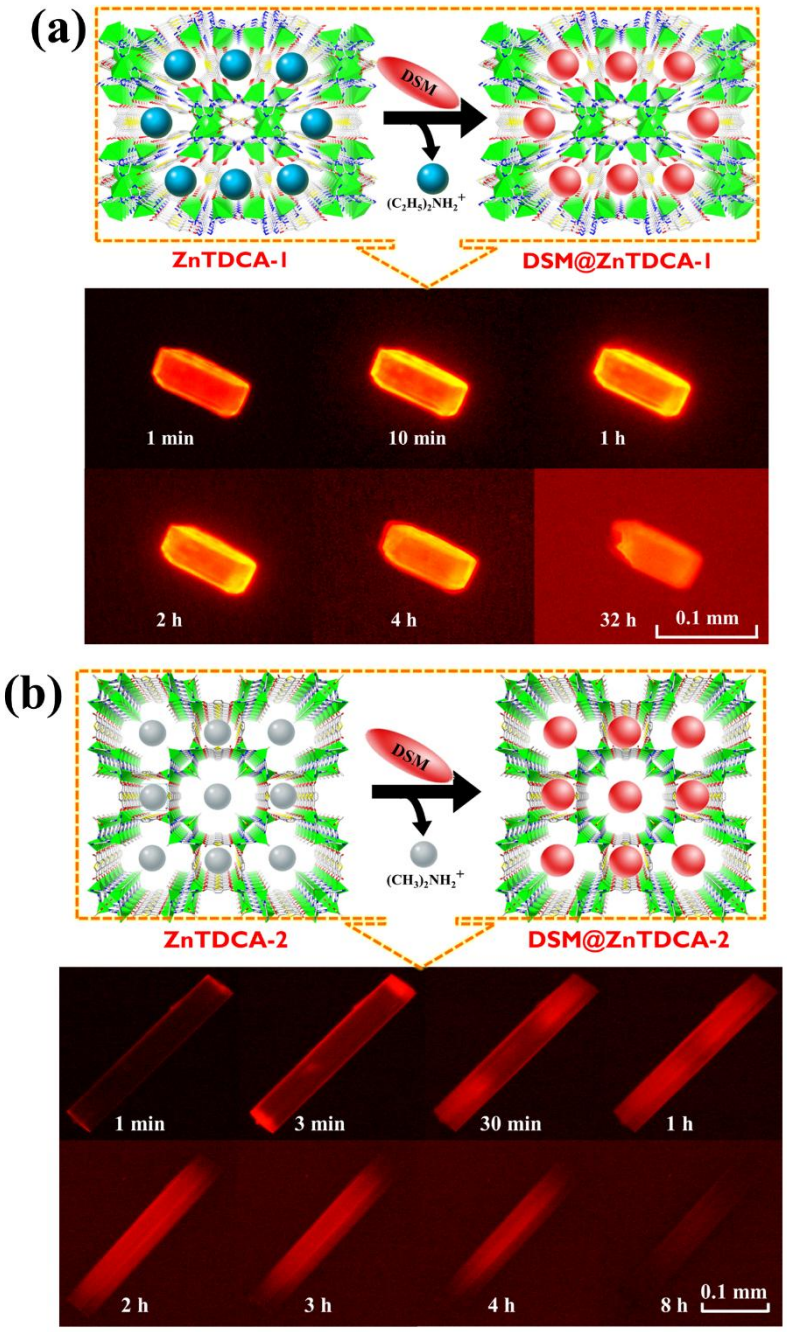

Fig. S21 Encapsulation of DSM into (a) ZnTDCA-1 and (b)ZnTDCA-2 and the corresponding fluorescent microscopic images evolution (in 1.00 mg/mL DSM solution)

DSM Release Experiments

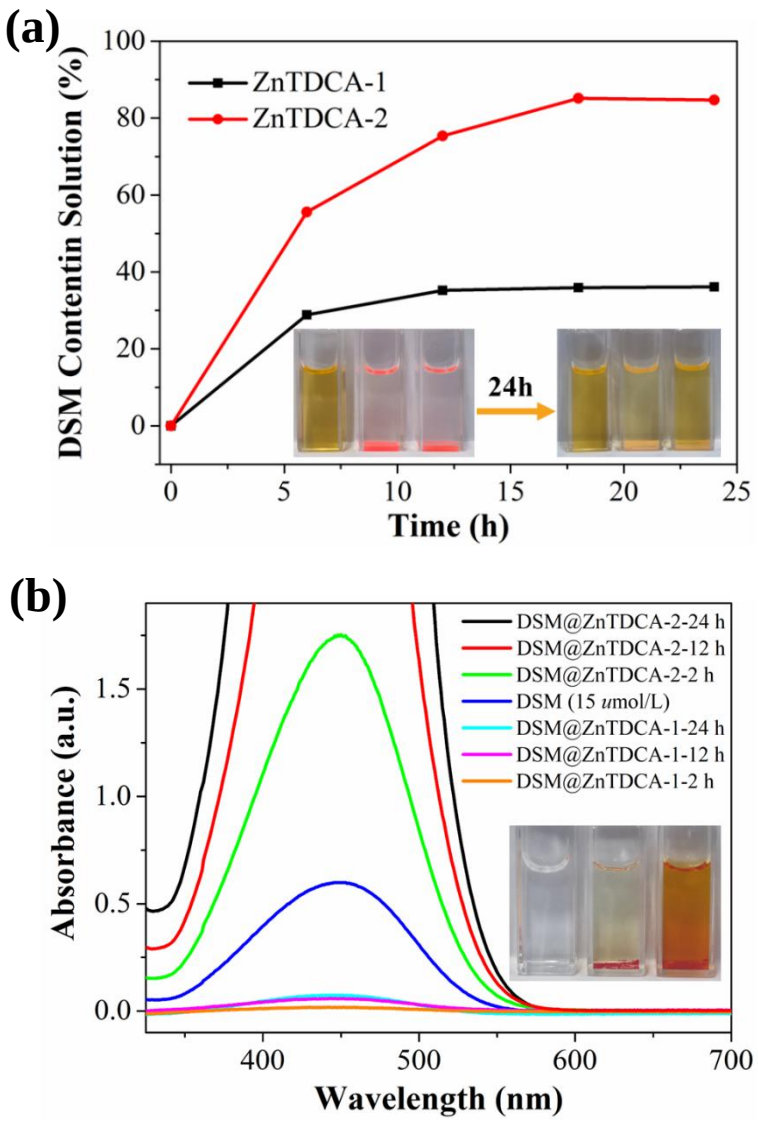

Fig. S22 (a) DSM percentages remained in solutions after being adsorbed into ZnTDCA-1 and ZnTDCA-2, the inner illustrations are photos of DSM/DMF blank solution (left), ZnTDCA-1 soaking in $Zn(NO_3)_2$/DMF solution (middle) and ZnTDCA-2 soaking in $Zn(NO_3)_2$/DMF solution (right) before and after 24 hours. (b) Absorption spectra of DSM solutions when 2 mg 0.78 wt% DSM@ZnTDCA-1 or 3.15 wt% DSM@ZnTDCA-2 were immersed in 2 mL PBS solutions for 2, 12, and 24 h. 15 *u*mol/L DSM/PBS was used as reference, the inner illustrations are photos of DSM/PBS blank solution (left), 0.78 wt% DSM@ZnTDCA-1 soaking in PBS solution (middle) and 3.15 wt% DSM@ZnTDCA-2 soaking in PBS solution (right) after 24 h.

Cell Culture and Cytotoxicity Experiments

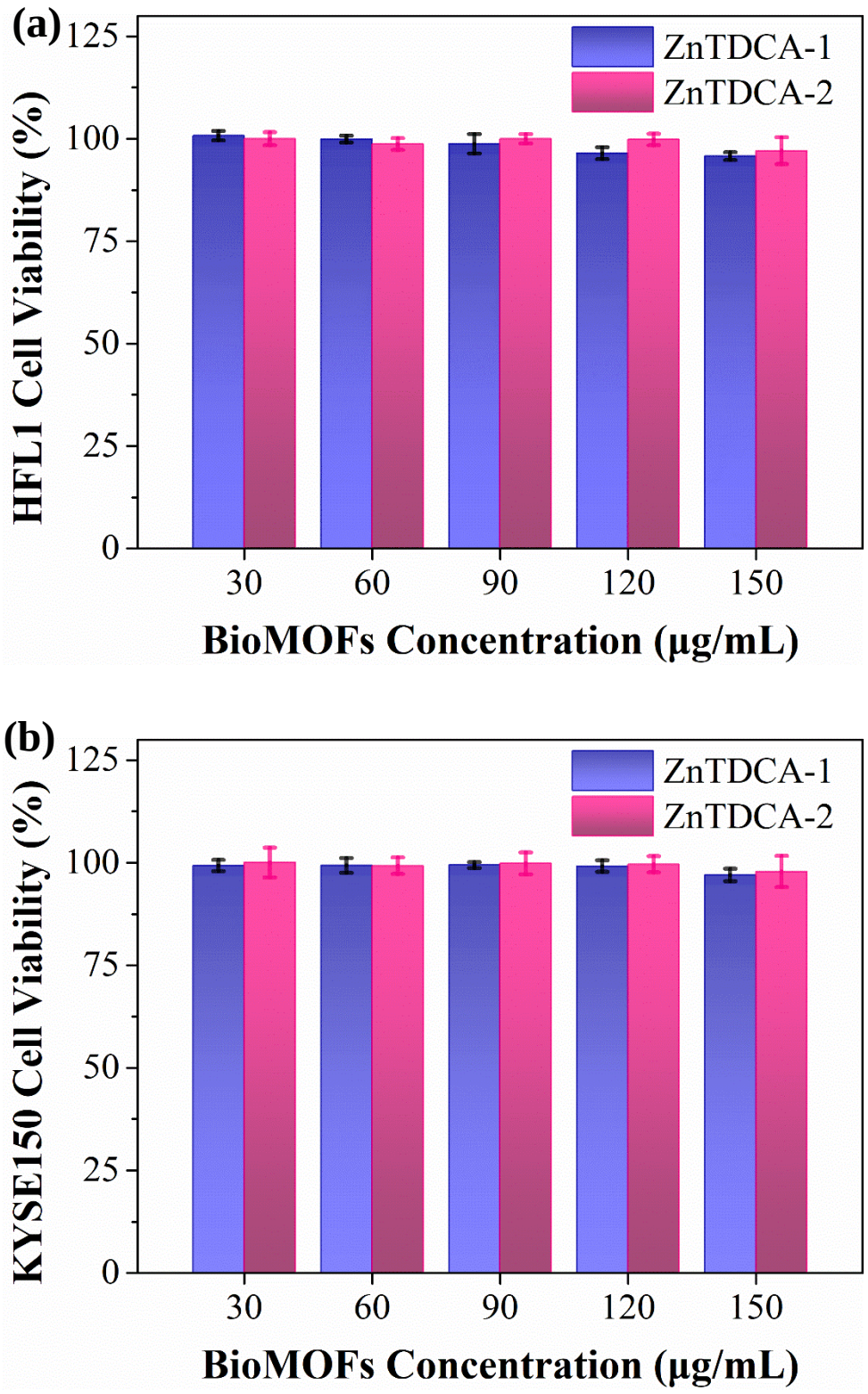

Fig. S23 HFL1(a) and KYSE150(b) cell viability after exposure to different concentration of ZnTDCA-1(royal) and ZnTDCA-2 (pink) for 48 h.

DFT Computation

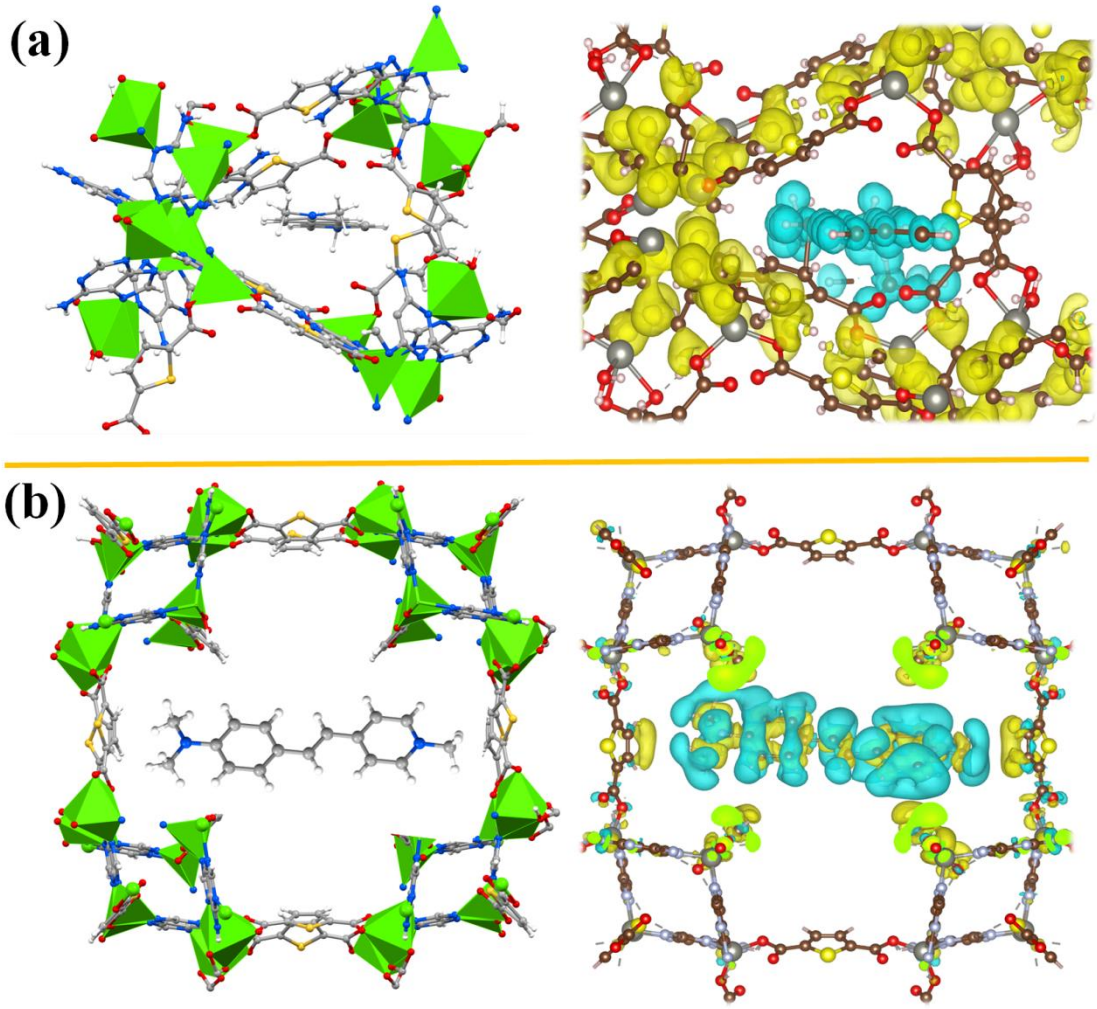

Fig. S24 Charge density difference for the host-guest interaction structures of (a) ZnTDCA-1 and (b) ZnTDCA-2, in which blue and yellow regions indicate electron depletion and accumulation, respectively.

References

1. G. M. Sheldrick, Crystal structure refinement with SHELXL. *Acta Cryst. C.* 2015, **71**, 3-8.
2. A. L. Spek, Single-crystal structure validation with the program PLATON. *J. Appl. Crystallogr.* 2003, **36**, 7-13.
3. O. Delgado-Friedrichs and M. O'Keeffe, Identification of and symmetry computation for crystal nets, *Acta Cryst. A*, 2003, **59**, 351-360.
4. V. A. Blatov, A. P. Shevchenko and D. M. Proserpio, Applied Topological Analysis of Crystal Structures with the Program Package ToposPro, *Cryst. Growth Des.*, 2014, **14**, 3576-3586.
5. V. A. Blatov, M. O'Keeffe and D. M. Proserpio, Vertex-, face-, point-, Schläfli-, and Delaney-symbols in nets, polyhedra and tilings: recommended terminology, *CrystEngComm*, 2010, **12**, 44-48.
6. M. O'Keeffe, M. A. Peskov, S. J. Ramsden and O. M. Yaghi, The Reticular Chemistry Structure Resource (RCSR) Database of, and Symbols for, Crystal Nets, *Acc. Chem. Res.*, 2008, **41**, 1782-1789. Online access: http://rcsr.net/
7. A. P. Shevchenko, A. A. Shabalin, I. Y. Karpukhin and V. A. Blatov, Topological representations of crystal structures: generation, analysis and implementation in the TopCryst system, *Sci. Technol. Adv. Mater.: Methods*, 2022, **2**, 250-265. Online access: https://topcryst.com/
8. H. Cai, L.-L. Xu, H.-Y. Lai, J.-Y. Liu, S. W. Ng and D. Li, A highly emissive and stable zinc(II) metal–organic framework as a host–guest chemopalette for approaching white-light-emission, *Chem. Commun.*, 2017, **53**, 7917-7920.
9. J. R. Lakowicz, Principles of Fluorescence Spectroscopy(3^{rd}), Springer, NewYork, 2016, 143.
10. E. A. Dolgopolova, D. E. Williams, A. B. Greytak, A. M. Rice, M. D. Smith, J. A. Krause and N. B. Shustova, A bio-inspired approach for chromophore communication: ligand-to-ligand and host-to-guest energy transfer in hybrid crystalline scaffolds. *Angew. Chem. Int. Ed.* 2015, **54**, 13639-13643.
11. H. Cai, W. Lu, C. Yang, M. Zhang, M. Li, C.-M. Che and D. Li, Tandem Förster Resonance Energy Transfer Induced Luminescent Ratiometric Thermometry in Dye-Encapsulated Biological Metal–Organic Frameworks, *Adv. Opt. Mater.*, 2019, **7**, 1801149.